In-medium *NN* cross sections determined from the nuclear stopping and collective flow in heavy-ion collisions at intermediate energies

Yingxun Zhang,[1,*] Zhuxia Li,[1,2,3,†] and Pawel Danielewicz[4]
[1]*China Institute of Atomic Energy, P.O. Box 275 (18), Beijing 102413, People's Republic of China*
[2]*Center of Theoretical Nuclear Physics, National Laboratory of Lanzhou Heavy Ion Accelerator, Lanzhou 730000, People's Republic of China*
[3]*Institute of Theoretical Physics, Chinese Academic of Science, Beijing 100080, People's Republic of China*
[4]*National Superconducting Cyclotron Laboratory, Michigan State University, East Lansing, Michigan 48824, USA*
(Received 1 September 2006; published 23 March 2007)

In-medium nucleon-nucleon scattering cross sections are explored by comparing results of quantum molecular dynamics simulations to data on stopping and on elliptic and directed flow in intermediate-energy heavy-ion collisions. The comparison points to in-medium cross sections which are suppressed at low energies but not at higher energies. Positive correlations are found between the degree of stopping and the magnitudes of elliptic and directed flows.

DOI: 10.1103/PhysRevC.75.034615 PACS number(s): 25.70.−z, 21.30.Fe, 21.65.+f, 24.10.Lx

One of the main goals of research in the area of heavy ion collisions (HICs) at intermediate energies has been the determination of bulk properties of nuclear matter, such as the nuclear equation of state (EoS). While a considerable progress [1–5] including that in subthreshold kaon production which provides complementary information on the EOS [6] has been reached in determining the EoS at supranormal densities, relying on reaction data, the uncertainties are still very large. To access the EoS, it is necessary to describe reaction observables [3–5], such as those quantifying the collective motion of nuclear matter, within reaction theory [1,2,7–11]. The transport models employed in the description of central reactions have included the quantum molecular dynamics approaches in its QMD [12,13] and ImQMD [14–16] (with Im for Improved) variants, as well as the Boltzmann-Uehling-Uhlenbeck (BUU) approaches [17–19]. The two main ingredients of the nuclear transport are the nucleonic mean fields and nucleon-nucleon binary scattering cross sections (NNCS). The employed cross sections affect virtually any observable from a central reactions and constraining those cross sections is essential for reducing the EoS uncertainties [9]. Also the in-medium cross sections are of interest for their own sake, as they underly the viscosity and other nuclear transport coefficients [20]. Best for constraining the cross sections are the stopping observables [21,22] that reflect the cross sections in the most direct manner. However, the correlation [21] with flow observables, such as used for determining the EoS, is also of interest. In this paper, for constraining the cross sections, we shall employ the ImQMD model [14–16].

Principally, within theory the mean field and cross sections of transport calculations should be linked to the same microscopic nucleon-nucleon interactions. In practice, this has turned out to be overly ambitious resulting in the phenomenological strategies in transport of varying independently the mean field, related to EoS, and the NNCS. Microscopically, far fewer calculations have been done of the in-medium cross-sections than of the EoS and of the mean fields. Specifically, the zero-temperature in-medium elastic NNCS (ENNCS) have been studied within the relativistic [23–25] and nonrelativistic Brueckner approaches [26,27]. In Refs. [24,25], employing the Brueckner relativistic approach, it was found that, compared to the free ENNCS, the in-medium ENNCS were suppressed at low relative momenta and less suppressed at higher relative momenta and even enhanced slightly depending on the medium density. The in-medium ENNCS have also been studied by using the closed time path Green's function (CTPGF) approach [28–31] employing, in particular, the QHD-I and QHD-II effective Lagrangians, with the mean field and in-medium ENNCS derived self-consistently for the same effective interaction. The latter studies [29–31] produced in-medium correction factors which were different for the cross sections of like, $\sigma^*_{\mathrm{nn,pp}}$ and unlike, σ^*_{np}, nucleons. Otherwise, the zero-temperature ENNCS from the Dirac-Brueckner [24,25] and CTPGF [29–31] have exhibited similar qualitative features but the results have differed in the details of their dependance on density and energy. The temperature dependence of the in-medium ENNCS has been investigated in [31] within the CTPGF approach and a general increase in the ENNCS with temperature was found. Elsewhere [32], though, difficulties have been pointed out in defining the cross sections within a nuclear medium. Those difficulties might relegate the cross sections utilized in transport to strictly phenomenological quantities. In the comparisons of nuclear reaction simulations to data, indeed, most often phenomenological cross section parametrizations have been employed, as, e.g., represented by the formula

$$\sigma^*_{\mathrm{NN}} = (1 - \eta\rho/\rho_0)\sigma^{\mathrm{free}}_{\mathrm{NN}}, \tag{1}$$

where $\eta = 0.2$ [22,25,33,34]. The in-medium ENNCS scaled by the effective mass, $\sigma^*_{\mathrm{NN}}/\sigma^{\mathrm{free}}_{\mathrm{NN}} = (m^*(\rho, p)/m)^2$ has also been employed in comparisons [35] to data from heavy-ion collisions (HIC). The latter scaling presumes that, for given

*Electronic address: zhyx@ciae.ac.cn
†Electronic address: lizwux@ciae.ac.cn

relative momenta, the matrix elements of interaction are not changed between the free space and medium.

The purpose of this work is to draw conclusions on the in-medium ENNCS using recent data on stopping and elliptic and directed flows, obtained with a good centrality selection, from collisions of Au+Au and other symmetric or near-symmetric systems [21,36,37]. For those data, a high degree of correlation was found between the degree of stopping and the strength of collective flow. In our investigations we rely on the recent version IMQMD05 of the IMQMD model [14–16].

Within the IMQMD05 model, the mean fields acting on nucleon wave packets are derived from an energy functional where the potential energy U includes the full Skyrme potential energy with just the spin-orbit term omitted:

$$U = U_\rho + U_{\rm md} + U_{\rm Coul}. \tag{2}$$

Here, $U_{\rm Coul}$ is the Coulomb energy, while the nuclear contributions can be represented in local form with $U_{\rho,{\rm md}} = \int {\rm d}^3 r u_{\rho,{\rm md}}$ and

$$\begin{aligned} u_\rho &= \frac{\alpha}{2}\frac{\rho^2}{\rho_0} + \frac{\beta}{\gamma+1}\frac{\rho^{\gamma+1}}{\rho_0^\gamma} + \frac{g_{\rm sur}}{2\rho_0}(\nabla\rho)^2 + \frac{g_{\rm sur,iso}}{\rho_0} \\ &\times [\nabla(\rho_{\rm n}-\rho_{\rm p})]^2 + (A\rho^2 + B\rho^{\gamma+1} + C\rho^{8/3})\delta^2 \\ &+ g_{\rho\tau}\frac{\rho^{8/3}}{\rho_0^{5/3}}, \end{aligned} \tag{3}$$

where $\delta = (\rho_{\rm n}-\rho_{\rm p})/(\rho_{\rm n}+\rho_{\rm p})$, $\rho = \rho_{\rm n}+\rho_{\rm p}$ and $\rho_{\rm n}$ and $\rho_{\rm p}$ are the neutron and proton densities, respectively. The energy associated with the mean-field momentum dependence may be represented as

$$\begin{aligned} u_{\rm md} &= \frac{1}{2\rho_0}\sum_{N_1,N_2={\rm n,p}}\frac{1}{16\pi^6}\int {\rm d}^3p_1 {\rm d}^3p_2 f_{N_1}(\mathbf{p}_1) f_{N_2}(\mathbf{p}_2) \\ &\times 1.57\,[\ln(1.+5.\times 10^{-4}(\Delta p)^2)]^2, \end{aligned} \tag{4}$$

where f_N are nucleon Wigner functions, $\Delta p = |\mathbf{p}_1 - \mathbf{p}_2|$, the energy is in MeV and momenta are in MeV/c; the resulting interaction between wave packets is such as in Ref. [38]. The coefficients utilized in Eq. (3) can be transcribed, see [16], onto those usually specified for the Skyrme interactions. In this work, the SkP and SLy7 Skyrme interactions are employed. Both of those interactions give rise to an incompressibilty of $K \sim 200$ MeV and produce an EOS consistent with the features of collective flow in HICs from Fermi to relativistic energies. However, the symmetry energies associated with those two interactions are different. It should be stressed that the expression for the energy (3) is more complete here than in the preceding Ref. [16].

Within this paper, three different phenomenological forms of in-medium ENNCS are utilized. The first set $\sigma_{\rm NN}^{*(1)}$ are the cross sections given by Eq. (1) with $\eta = 0.2$ and with the free cross sections described in terms of the parametrization of Ref. [39]. The second set $\sigma_{\rm NN}^{*(2)}$ are cross sections calculated within the CTPGF approach of Ref. [30], following the QHD-II Lagrangian. For calculational convenience, within IMQMD the formula (1) is, though, employed with η made dependent on density and energy and its dependence fitted

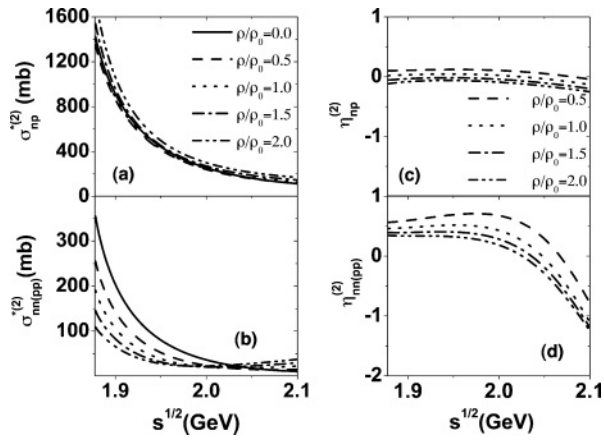

FIG. 1. Energy dependence of in-medium cross sections $\sigma_{\rm np}^{*(2)}$ and $\sigma_{\rm nn,pp}^{*(2)}$, in panels (a) and (b), and of the suppression parameters $\eta_{\rm np}^{(2)}$ and $\eta_{\rm nn,pp}^{(2)}$, in panels (c) and (d), at selected densities. The cross sections have been obtained within the CTPGF approach with QHD-II effective Lagrangian.

to the CTPGF results. For reference, in Fig. 1 we present both the cross sections, $\sigma_{\rm np}^{*(2)}$ and $\sigma_{nn,pp}^{*(2)}$ in panels (a) and (b), and the suppression parameters, $\eta_{\rm np}^{(2)}$ and $\eta_{nn(pp)}^{(2)}$ in panels (c) and (d), as a function of c.m. energy $\sqrt{s}$ at different densities. One can see that $\sigma_{\rm np}^{*(2)}$ changes little with density and is nearly the same as in free space. On the other hand, the cross section $\sigma_{\rm nn,pp}^{*(2)}$ tends to be suppressed at lower energies, $\sqrt{s} \lesssim 2.05$ GeV and enhanced at higher. Differences in the features of the two cross sections are associated with the differences between the $T = 0$ and the $T = 1$ channels and, in particular, presence of a low-energy resonance in the $T = 1$ channel and effects of ρ exchange. The third set constitutes and ad hoc parametrization, inspired by the CTPGF results, aiming at the description of the excitation function for elliptic flow in the midrapidity region of $|y_{\rm c.m.}/y_{\rm c.m.}^{\rm beam}| < 0.1$ in Au+Au collisions [16]. In that parametrization, the common cross-section modification parameter, $\eta^{(3)} = \eta_{\rm np}^{(3)} = \eta_{\rm nn(pp)}^{(3)}$, depends on the beam energy for reaction, $E_{\rm beam}$, in the following manner: $\eta^{(3)} = 0.2$ for $E_{\rm beam} < 150A$ MeV, $\eta^{(3)} = 0$ for $150A$ MeV $< E_{\rm beam} < 200A$ MeV, $\eta^{(3)} = -0.2$ for $200A$ MeV $< E_{\rm beam} < 400A$ MeV, and $\eta^{(3)} = -0.4$ for $400A$ MeV $< E_{\rm beam}$. In this paper, we actually confine ourselves to the HIC energy range of $E_{\rm beam} < 400A$ MeV since, on one hand, our model is nonrelativistic and, on the other, higher energies require a consideration of the inelastic cross section that we are not prepared to carry out at this moment.

First, we investigate the impact of in-medium NNCS onto the model predictions for elliptic and directed flows in Au+Au collisions. Excitation functions for both flow observables have been determined experimentally [21,36,37]. The top panels in Fig. 2 show the excitation function of the elliptic flow parameter v_2 for $Z \leqslant 2$ particles in the midrapidity region of $|y_{\rm c.m.}/y_{\rm c.m.}^{\rm beam}| < 0.1$. The v_2 values have been obtained using the rotated frame [36]. The bottom panels in Fig. 2 show the excitation function of maximal scaled directed flow in Au+Au collisions at $b \simeq 5$ fm ($b/b_{\rm max} \sim 0.38$). The scaled flow is defined with [21] $p_{x\rm dir}^{(0)} = p_{x\rm dir}/u_{\rm c.m.}^{\rm beam}$,

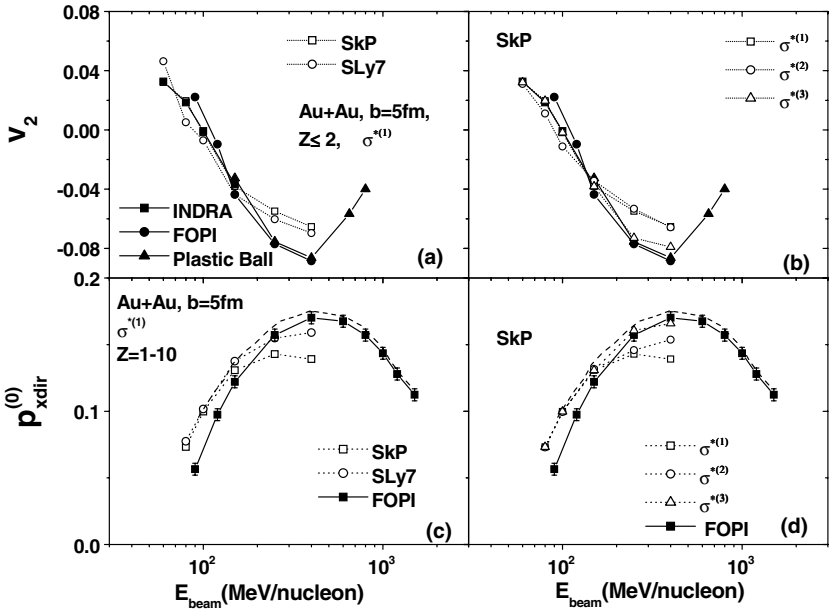

FIG. 2. Flow excitation functions in Au+Au collisions. The top panels display midrapidity elliptic flow. The bottom panels display maximal scaled directed flow. The data are represented by solid symbols and calculations by open symbols. Lines generally merely guide the eye, except for the dashed lines in the bottom panels. In these cases, the dashed lines illustrate the change in the directed flow data after applying the correction for reaction-plane fluctuation. The left panels in the figure illustrate the sensitivity of calculations to the employed mean field. The right panels illustrate the sensitivity of calculations to in-medium cross sections.

where $u^{\rm beam}_{\rm c.m.} = \gamma^{\rm beam}_{\rm c.m.}\beta^{\rm beam}_{\rm c.m.}$ and $p_{x\rm dir} = \sum {\rm sgn}(y) Z u_x / \sum Z$. The sums in the directed flow extend over all particles with charge number $Z \leqslant 10$. The data and calculations are represented in Fig. 2 with closed and open symbols, respectively. Lines generally merely guide the eye, except for the dashed lines in the bottom panels. In these cases, the dashed lines illustrate the change in the directed flow data after applying the correction for reaction-plane fluctuation. The calculations in the left panels of Fig. 2 have been carried out with the SkP and SLy7 mean fields and $\sigma^{*(1)}$ cross sections. The differences between the calculated v_2 values in the panel (a) of Fig. 2 are limited and can be due to the difference in the symmetry energy between the two mean-field models. Notably, there are some differences between the data sets in the figure too. One more significant difference which develops between the calculations for different mean fields in Fig. 2 is in $p^{(0)}_{x\rm dir}$ in panel (c) at $E_{\rm beam} > 150A$ MeV. The calculations in the right panels of Fig. 2 are for the SkP mean field in combination with the three different cross-section models. The sensitivity of flow to the cross sections is similar to the sensitivity to the mean-field models. It is limited on absolute scale but gets more enhanced at higher energies. The deviations between the models are similar to the deviations of models from data. From the presented mean-field and cross-section combinations, the SkP mean-field in combination with $\sigma^{*(3)}$ cross sections describe the flow data best.

We next turn to the impact of NNCS on nuclear stopping. Recently, in the experiment [21], the ratio of the rapidity variance in the transverse direction to the rapidity variance in the longitudinal direction, *vartl*, has been used a measure of the nuclear stopping. The longitudinal rapidity for the ratio is defined in the standard manner in the c.m. system. The transverse rapidity is defined by replacing the longitudinal direction in the definition with a random transverse direction. Figure 3 shows a variety of results pertinent to *vartl*. The results are for charged particles with $Z = 1$–6 from central collisions of symmetric or near-symmetric systems, with the contributions of different particles weighted with Z. The panels (a) and (b) in Fig. 3 show calculated distributions in longitudinal and transverse rapidities in 400A MeV Au+Au collisions at $b/b_{\rm max} < 0.15$. The corresponding *vartl* values for different calculations are quoted in those panels. The panel (c) compares chosen calculated Au+Au excitation functions for *vartl* to data. Finally, the panel (d) compares the calculated dependence of *vartl* on system charge to data at 400A MeV.

From the different panels of Fig. 3, the panel (a) tests the sensitivity of the calculated rapidity distributions to a utilized mean field. It is apparent that that sensitivity is quite weak. Quantitatively, when switching from the SkP to Sly7 mean field, *vartl* increases just by 0.015, i.e., relative 2%. The panel (b) next tests the sensitivity of the calculated rapidity distributions to a utilized cross section. The sensitivity is much greater here, with *vartl* changing by 0.22 or 32% when switching from the $\sigma^{*(1)}$ to $\sigma^{*(3)}$ cross section. Thus, there is a good chance to restrict the in-medium cross sections using measured *vartl* but less chance to restrict the mean field. What is important in Fig. 3(b) is that the larger the cross section in the given energy region the more similar are the transverse and longitudinal distributions and the larger the corresponding *vartl* value. The panels (c) and (d) compare to data the results obtained with the SkP mean field and two of the in-medium cross sections, $\sigma^{*(1)}$ and $\sigma^{*(3)}$. At lower energies a semiquantitative agreement with the Au+Au data is found and there the cross sections coincide. However, at higher energies the Au+Au data favor $\sigma^{*(3)}$ NNCS. The $\sigma^{*(1)}$ NNCS appears excessively reduced and this also concerns $\sigma^{*(2)}$ given the 400A MeV *vartl* value of 0.805 in the panel (b). Looking next at the system charge dependence of *vartl* in the panel (d), it appears that an optimal in-medium cross at 400A MeV could be a bit lower than $\sigma^{*(3)}$. Of the three cross sections, nonetheless, $\sigma^{*(3)}$ compares best with the data.

Experimentally, the values of *vartl* maximize at $E_{\rm beam} \sim$ 400A MeV and so do the values of $p^{(0)}_{x\rm dir}$. At the same time, the elliptic flow values minimize in this energy region [36]. If the

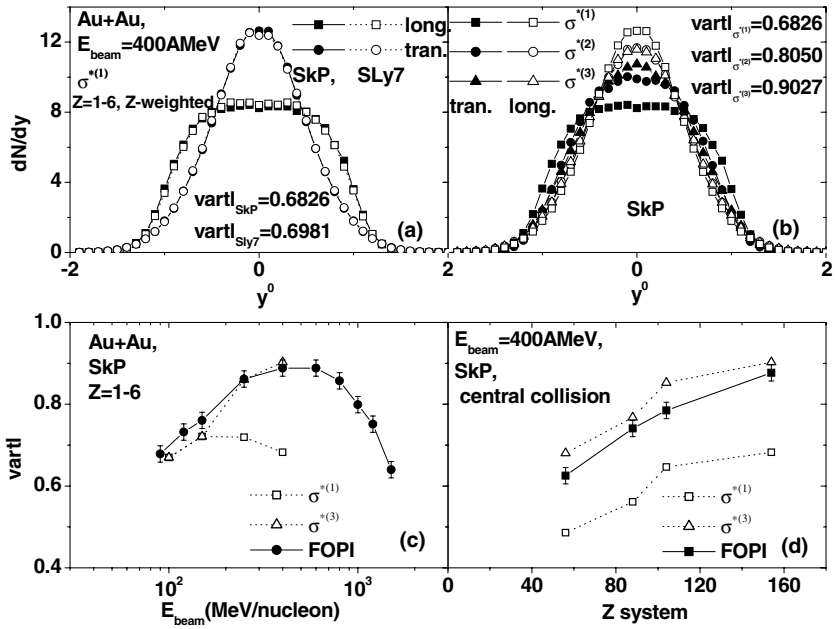

FIG. 3. Comparison of characteristics of central colliding systems in the longitudinal and transverse rapidities. Panels (a) and (b) display the calculated rapidity distributions of particles from central ($b/b_{\max} < 0.15$) $400A$ MeV Au+Au collisions and illustrate, respectively, the sensitivity of calculations to the mean field and to the cross sections. The rapidities are normalized to the beam c.m. rapidity. Panels (c) and (d) display the calculated and measured dependencies of the variance ratio *vartl*, respectively, on energy for the Au+Au collisions and on net system charge at collision energy $400A$ MeV. The data are from FOPI Collaboration [21]. The calculations have been done for the SkP mean field combined with either $\sigma^{*(1)}$ or $\sigma^{*(3)}$ cross sections.

values of *vartl* at different energies for the Au+Au system are considered simultaneously with the values of maximal scaled directed flow, a positive relatively narrow correlation is found between the observables [21]. Importantly, that correlation is between observables determined, on one hand, in the most central $b/b_{\max} < 0.15$ collisions and, on the other, the semicentral $b/b_{\max} \sim 0.38$ collisions. This suggests, from the experimental side, that both observables probe bulk nuclear properties which come into play at specific densities and excitations reached at a particular beam energy. Between the *vartl* and v_2 values, again determined at different centralities, a negative correlation is expected. Interestingly, when other symmetric or near-symmetric systems are considered, and specifically Ni+Ni, Ru+Ru and Xe+Cs, the resulting correlations appear to extend the correlation lines found for Au+Au, see Fig. 4, with the left panel (a) showing the $p^{(0)}_{x\,\mathrm{dir}}$-*vartl* correlation and the right panel (b) the v_2-*vartl* correlation. The system systematics appears further to underscore, from the experimental side, that bulk nuclear properties get tested by the observables.

It is obviously important to find out whether the IMQMD05 model produces correlations comparable to those measured and whether the calculated and measured correlations agree quantitatively. Figures 4(a) and 4(b) show the correlation of maximal $p^{(0)}_{\mathrm{xdir}}$ and v_2 with *vartl*, respectively. All of these results are for the reaction systems Ni+Ni, Ru+Ru, Xe+Cs, Au+Au at $E_{\mathrm{beam}} = 250, 400A$ MeV. While the data are represented with crosses and stars in Fig. 4, the calculations are represented with planar-figure symbols. For each of the represented cross sections, i.e., either $\sigma^{*(1)}$ represented by open symbols, or $\sigma^{*(3)}$ represented by closed symbols, in combination with the SkP mean field, the calculations produce approximate correlation lines in the planes of flow vs *vartl*, with positive slope in the case of $p^{(0)}_{x\,\mathrm{dir}}$ and negative in the case of v_2. One of the calculated correlations, v_2-*vartl* for $\sigma^{*(1)}$, is somewhat broader than the others. To aid the eye, the correlation areas for $\sigma^{*(1)}$ are additionally marked with shadowing. Within the reaction simulations, the correlations between stopping and flow may be primarily associated with the collisions governed by cross sections. The greater the momentum transfer in collisions the higher the stopping. However, the occurring local randomization due to collisions also enhances hydrodynamic behavior and, thus, enhances the magnitude of flow observables. From the calculated correlations in Fig. 4, only the two obtained using $\sigma^{*(3)}$ reasonably agree with data. Notably, with the stopping and flow

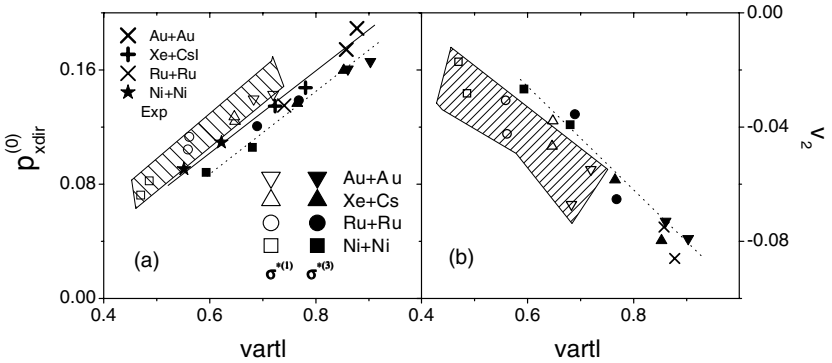

FIG. 4. Correlation between *vartl* and flow observables: $p^{(0)}_{x\,\mathrm{dir}}$ in the panel (a) and v_2 in (b). Both the data [21,36] and calculations are represented.

observables simultaneously growing in magnitude with collision number, the correlation lines associated with the different cross sections could have actually coincided. However, *vartl* and flow observables depend on interactions differently. The *vartl* observable exhibits a strong dependence on cross sections and little on mean field, while flow observables depend to a comparable extent on cross sections and mean field. As a result, the correlation lines can end up being different for the different cross sections.

In summary, within the IMQMD05 model we have investigated the impact of in-medium NNCS and mean fields on stopping and flow in HICs at intermediate energies. The *vartl* observable, quantifying the stopping, depends strongly on NNCS and little on mean-field details. On the other hand, the v_2 and $p^{(0)}_{x\mathrm{dir}}$ flow observables depend comparably on uncertainties in the NNCS and mean fields. Within the upper range of the energies we have investigated, both the common NNCS parametrization represented by $\sigma^{*(1)}$ and the CTPGF cross section represented by $\sigma^{*(2)}$ appeared excessively reduced in the medium to produce observed *vartl* values [21]. Also the magnitudes of flow observables calculated for those cross sections turned out to be low compared to the experiment. The agreement between the data and calculations gets much improved when employing an ad hoc cross section parametrization guided by CTPGF and represented by $\sigma^{*(3)}$. For that parametrization the nucleon-nucleon cross sections in the medium are suppressed at low energies and enhanced at higher energies, i.e., the extracted in-medium nucleon-nucleon cross sections depend on both density and energy. In this respect it is also in agreement with the prediction of [24,25]. The results clearly do not represent the last word on in-medium cross sections as medium-variation of the cross sections in the parametrization has been clearly oversimplified. From the side of observables, those that we examined do not strongly differentiate between the like and unlike nucleon cross sections.

ACKNOWLEDGMENTS

This work was supported by the National Natural Science Foundation of China under Grant Nos. 10175093, 10675172 and 10235030, by the Major State Basic Research Development Program under Contract No. G20000774 and by the U.S. National Science Foundation, Grant No. PHY-0555893.

[1] P. Danielewicz, R. Lacey, and W. G. Lynch, Science **298**, 1592 (2002).
[2] C. Fuchs, Prog. Part. Nucl. Phys. **56**, 1 (2006).
[3] M. Demoulins *et. al.*, Phys. Lett. **B241**, 476 (1990).
[4] H. H. Gutbrod, K. H. Kampert, B. Kolb *et al.*, Phys. Lett. **B216**, 267 (1989); Phys. Rev. C **42**, 640 (1990).
[5] W. Reisdorf and H. G. Ritter, Annu. Rev. Nucl. Part. Sci. **47**, 663 (1997).
[6] C. Sturm, I. Böttcher, M. Debowski *et al.*, Phys. Rev. Lett. **86**, 39 (2001); C. Fuchs, A. Faessler, E. Zabrodin, and Y. M. Zheng, *ibid.* **86**, 1974 (2001); C. Hartnack, H. Oeschler, and J. Aichelin, Phys. Rev. Lett. **96**, 012302 (2006).
[7] H. Stöcker and W. Greiner, Phys. Rep. **137**, 277 (1986).
[8] C. Gale, G. M. Welke, M. Prakash, S. J. Lee, and S. Das Gupta, Phys. Rev. C **41**, 1545 (1990).
[9] Q. Pan and P. Danielewicz, Phys. Rev. Lett. **70**, 2062 (1993); **70**, 3523 (1993).
[10] B. A. Li and A. Sustich, Phys. Rev. Lett. **82**, 5004 (1999).
[11] H. Zhou, Z. Li, and Y. Zhuo, Phys. Rev. C **50**, R2664 (1994); H. Zhou, Z. Li, Y. Zhuo, and G. Mao, Nucl. Phys. **A580**, 627 (1994).
[12] J. Aichelin, A. Rosenhauer, G. Peilert, H. Stoecker, and W. Greiner, Phys. Rev. Lett. **58**, 1926 (1987); J. Aichelin and H. Stöcker, Phys. Lett. **B176**, 14 (1986).
[13] C. Hartnack, Z. Li, L. Neise *et al.*, Nucl. Phys. **A495**, 303 (1989).
[14] N. Wang, Z. Li, and X. Wu, Phys. Rev. C **65**, 064608 (2002); N. Wang, Z. Li, X. Wu, J. Tian, Y. X. Zhang, and M. Liu, *ibid.* **69**, 034608 (2004).
[15] Y. Zhang and Z. Li, Phys. Rev. C **71**, 024604 (2005).
[16] Y. Zhang and Z. Li, Phys. Rev. C **74**, 014602 (2006).
[17] G. F. Bertsch, H. Kruse, and S. D. Gupta, Phys. Rev. C **29**, 673 (1984).
[18] J. Aichelin and G. F. Bertsch, Phys. Rev. C **31**, 1730 (1985).
[19] Q. Li, J. Q. Wu, and C. M. Ko, Phys. Rev. C **39**, 849 (1989).
[20] L. Shi and P. Danielewicz, Phys. Rev. C **68**, 064604 (2003).
[21] W. Reisdorf *et al.* (FOPI Collaboration), Phys. Rev. Lett. **92**, 232301 (2004).
[22] D. Persram and C. Gale, Phys. Rev. C **65**, 064611 (2002).
[23] B. ter Haar and R. Malfliet, Phys. Rev. C **36**, 1611 (1987).
[24] G. Q. Li and R. Machleidt, Phys. Rev. C **48**, 1702 (1993).
[25] C. Fuchs, A. Faessler, and M. Al-Shabshiry, Phys. Rev. C. **64**, 024003 (2001); T. Gaitanos, C. Fuchs, and H. H. Wolter, Phys. Lett. **B609**, 241 (2005).
[26] M. Kohno, M. Higashi, Y. Watanabe, and M. Kawai, Phys. Rev. C **57**, 3495 (1998).
[27] H. J. Schulze, A. Schnell, G. Röpke, and U. Lombardo, Phys. Rev. C **55**, 3006 (1997).
[28] W. H. Dickhoff, C. C. Gearhart, E. P. Roth, A. Polls, and A. Ramos, Phys. Rev. C **60**, 064319 (1999).
[29] G. Mao, Z. Li, Y. Zhuo, Y. Han, and Z. Yu, Phys. Rev. C **49**, 3137 (1994).
[30] Q. Li, Z. Li, and G. Mao, Phys. Rev. C **62**, 014606 (2000).
[31] Q. Li, Z. Li, and E. Zhao, Phys. Rev. C **69**, 017601 (2004).
[32] W. H. Dickhoff, Phys. Rev. C **58**, 2807 (1998).
[33] D. Klakow, G. Welke, and W. Bauer, Phys. Rev. C **48**, 1982 (1993).
[34] P. Danielewicz, Nucl. Phys. **A673**, 375 (2000).
[35] B.-A. Li and L. W. Chen, Phys. Rev. C **72**, 064611 (2005).
[36] J. Lukasik, G. Auger, M. L. Begemann-Blaich *et al.*, Phys. Lett. **B608**, 223 (2005).
[37] A. Andronic, G. Stoicea, M. Petrovici, V. Simion *et al.*, Nucl. Phys. **A679**, 765 (2001); A. Andronic, V. Barret, Z. Basrak, N. Bastid *et al.*, Phys. Lett. **B612**, 173 (2005).
[38] J. Aichelin, A. Rosenhauer, G. Peilert, H. Stöker, and W. Greiner, Phys. Rev. Lett. **58**, 1926 (1987).
[39] J. Cugnon, D. L'Hôte, and J. Vandermeulen, Nucl. Instrum. Methods Phys. Res. B **111**, 215 (1996).